
AutoQD: Automatic Discovery of Diverse Behaviors with Quality-Diversity Optimization

Saeed Hedayatian

Department of Computer Science
University of Southern California
Los Angeles, CA 90089
saeedhed@usc.edu

Stefanos Nikolaidis

Department of Computer Science
University of Southern California
Los Angeles, CA 90089
nikolaid@usc.edu

Abstract

Quality-Diversity (QD) algorithms have shown remarkable success in discovering diverse, high-performing solutions, but rely heavily on hand-crafted behavioral descriptors that constrain exploration to predefined notions of diversity. Leveraging the equivalence between policies and occupancy measures, we present a theoretically grounded approach to automatically generate behavioral descriptors by embedding the occupancy measures of policies in Markov Decision Processes. Our method, AutoQD, leverages random Fourier features to approximate the Maximum Mean Discrepancy (MMD) between policy occupancy measures, creating embeddings whose distances reflect meaningful behavioral differences. A low-dimensional projection of these embeddings that captures the most behaviorally significant dimensions is then used as behavioral descriptors for off-the-shelf QD methods. We prove that our embeddings converge to true MMD distances between occupancy measures as the number of sampled trajectories and embedding dimensions increase. Through experiments in multiple continuous control tasks we demonstrate AutoQD’s ability in discovering diverse policies without predefined behavioral descriptors, presenting a well-motivated alternative to prior methods in unsupervised Reinforcement Learning and QD optimization. Our approach opens new possibilities for open-ended learning and automated behavior discovery in sequential decision making settings without requiring domain-specific knowledge.

1 Introduction

Traditional optimization methods, focused solely on finding optimal solutions, often fail to capture the rich diversity of possible solutions that could be valuable in different contexts. Quality-Diversity (QD) optimization addresses this limitation by generating collections of solutions that are both high-performing and behaviorally diverse [9, 32]. This approach has demonstrated success across different domains including robot locomotion [10, 8], game level and scenario generation [19, 2], protein design [3], and even image generation [15].

Building on these successful applications, we focus on sequential decision-making tasks where we seek diverse and high-quality policies, a setting commonly referred to as Quality-Diversity Reinforcement Learning (QD-RL) [39, 27, 31]. Here, the importance of behavioral diversity stems from two key considerations. First, diverse policies provide robustness against changing conditions—when one policy fails, alternatives with different behavioral characteristics might succeed. Second, diversity is crucial for open-ended learning, where the goal extends beyond solving predefined problems to continually discovering novel capabilities and behaviors [25]. This is particularly relevant for developing autonomous systems that can systematically explore their capabilities, adapt to unforeseen

circumstances, and potentially discover unexpected but useful behaviors that human designers might not have anticipated.

A fundamental limitation of QD algorithms, particularly challenging in sequential decision-making tasks, is their reliance on hand-crafted *behavioral descriptors* (BDs). Behavioral descriptors are functions that map policies to low-dimensional vectors characterizing their behavior. For example, when designing controllers for a bipedal robot, researchers typically define BDs based on foot contact patterns, which allows them to characterize behaviors such as walking, jumping, and hopping. Hand-crafting BDs require substantial domain knowledge, which becomes increasingly difficult as task complexity grows. Furthermore, they inherently constrain the diversity of discovered policies to variations along predefined dimensions, potentially missing interesting behavioral variations [7].

In this paper, we present a theoretically principled approach to automatically generating behavioral descriptors. Our method is based on the concept of occupancy measures from reinforcement learning theory, which represents the expected discounted visitation frequency of state-action pairs when following that policy. Crucially, there exists a one-to-one correspondence between policies and their occupancy measures [33], making them ideal representations of behaviors as they fully characterize a policy. This fact differentiates our method from prior work in QD that focus on learning representations through optimizing proxy objectives such as state reconstruction [7] to define BDs, and a wide range of other methods from the RL literature that typically use information theoretic objectives to train a fixed number of policies to be maximally different or distinguishable [11, 24].

Our key insight is that by embedding occupancy measures into finite-dimensional vector spaces where distances approximate the Maximum Mean Discrepancy (MMD) between the occupancy measures, we can create behaviorally meaningful representations. These representations can then be further reduced to lower-dimensional behavioral descriptors for QD optimization.

Our approach, which we call AutoQD, addresses several limitations of existing QD methods. It does not require manual specification of behavioral descriptors and can potentially discover unexpected behavioral variations. Furthermore, its seamless integration with existing QD algorithms allows us to discover thousands of policies covering a continuous behavioral space.

Our main contributions are: (1) Developing a method to efficiently embed occupancy measures of policies from sampled trajectories (Sec. 3.1). (2) Formally showing how the distances between these embeddings approximate the true MMD distances between occupancy measures (Theorem 1). (3) Proposing an iterative algorithm that alternates between QD optimization and refinement of behavioral descriptors through dimensionality reduction (Sec. 3.2). (4) Demonstrating empirically that our approach discovers diverse, high-performing policies without requiring hand-crafted descriptors (Sec. 4).

2 Background

2.1 Markov decision processes and policy optimization

Following the established terminology in RL, we consider environments modeled as Markov Decision Processes (MDPs), defined by the tuple $(\mathcal{S}, \mathcal{A}, P, R, \gamma)$, where \mathcal{S} is the state space, \mathcal{A} is the action space, $P(s'|s, a)$ is the transition probability, $R(s, a)$ is the reward function, and $\gamma \in (0, 1)$ is the discount factor. A policy π is a function of the state, either deterministic ($\pi : \mathcal{S} \rightarrow \mathcal{A}$) or stochastic ($\pi : \mathcal{S} \rightarrow \Delta(\mathcal{A})$) representing an agent. In standard reinforcement learning, the goal is to find a policy that maximizes the expected discounted return $J(\pi) = \mathbb{E}_\pi[\sum_{t=0}^{\infty} \gamma^t R(s_t, a_t)]$.

A key concept in RL is the occupancy measure, which arises naturally in the study of the solutions to MDPs. For a policy π , its occupancy measure ρ^π is a distribution over state-action pairs defined as:

$$\rho^\pi(s, a) = (1 - \gamma) \sum_{t=0}^{\infty} \gamma^t P(S_t = s, A_t = a | \pi) \quad (1)$$

where $P(S_t = s, A_t = a | \pi)$ is the probability of visiting state-action pair (s, a) at time t when following policy π . The occupancy measure is fundamental to reinforcement learning as it captures the long-term visitation frequencies of state-action pairs under a policy, and many quantities of interest (including the expected return) can be expressed as expectations under this measure. Importantly, there

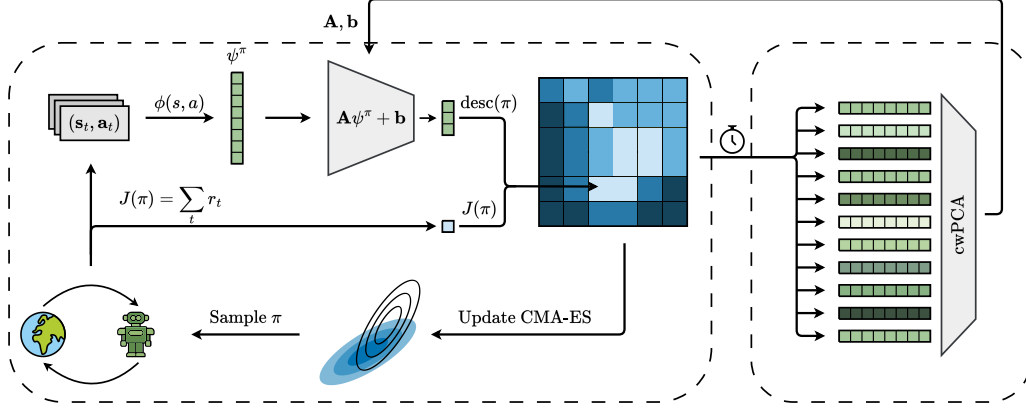


Figure 1: **Overview of AutoQD.** *Left:* Policy parameters are sampled from a CMA-ES instance and evaluated in the environment. The collected trajectories are embedded via a random Fourier features map ϕ to produce the policy embedding ψ^π , which is then projected to a low-dimensional descriptor using the affine map $\mathbf{A}\psi^\pi + \mathbf{b}$. The policy is added to the archive based on its return $J(\pi)$ and descriptors $\text{desc}(\pi)$, and CMA-ES updates its distribution based on the improvement made to the archive. *Right:* Periodically, embeddings from the archive are used to update \mathbf{A} and \mathbf{b} via calibrated, weighted PCA (cwPCA).

exists a one-to-one correspondence between policies and their occupancy measures (see Sec. 6.9.1 of [33]), making occupancy measures a complete characterization of policy behavior.

2.2 Quality-Diversity optimization

Quality-Diversity (QD) optimization aims to discover a collection of solutions that are both high-performing and behaviorally diverse. Unlike traditional optimization, which focuses on a single optimal solution, QD maintains an archive \mathbb{A} of solutions, each associated with both a performance measure and a behavioral descriptor. In QD reinforcement learning (QD-RL), a solution is the parameters of a policy π , typically represented as a neural network. The performance of a policy is its expected return, $J(\pi) = \mathbb{E}_\pi[\sum_{t=0}^{\infty} \gamma^t R(s_t, \mathbf{a}_t)]$, which we refer to as the *fitness*. A *behavioral descriptor* is a function $\text{desc} : \Pi \rightarrow \mathcal{B}$ that maps policies to a behavior space $\mathcal{B} \subseteq \mathbb{R}^k$. The goal of QD optimization is to find, for each behavior vector $\mathbf{b} \in \mathcal{B}$, a policy $\pi_{\mathbf{b}}$ that satisfies $\text{desc}(\pi_{\mathbf{b}}) = \mathbf{b}$ and maximizes the objective among all such policies. In practice, the behavior space \mathcal{B} is divided into a finite number of cells, called an *archive* \mathbb{A} with the QD goal being to fill each cell with the best solution. This objective is formalized by the *QD score*, defined as $\text{QDScore}(\mathbb{A}) = \sum_{\pi \in \mathbb{A}} J(\pi)$, which is the total fitness of all policies in the archive (In domains where the objective can be negative, a positive offset is added to all objectives to ensure that discovering more policies is not penalized by QD score). QD algorithms employ various optimization techniques including random mutations [9], evolutionary strategies [14], and gradient-based methods [27] to maximize this score.

In this work, we use CMA-MAE [13], which applies the Covariance Matrix Adaptation Evolution Strategy (CMA-ES) [23] to QD optimization. CMA-MAE runs multiple CMA-ES optimizers in parallel, each maintaining a Gaussian distribution over policy parameters. In each iteration, we sample a batch of policies from the Gaussian, evaluate their fitness, and map them into the archive via their behavioral descriptors. The algorithm then ranks the policies based on their improvement to the archive and uses this ranking to update the parameters of CMA-ES. This iterative update implicitly performs natural gradient ascent on (a reformulation of) the QD score [12], enabling efficient optimization of both quality and diversity.

2.3 Maximum mean discrepancy

To quantify the differences between policy behaviors, we turn to the *Maximum Mean Discrepancy* (MMD), a metric for comparing probability distributions. Intuitively, MMD measures the difference of two distributions by comparing statistics of their samples. Given two distributions P and Q over a

space \mathcal{X} , and a feature map $\phi : \mathcal{X} \rightarrow \mathbb{R}^D$, the MMD is defined as:

$$\text{MMD}(P, Q) = \|\mathbb{E}_{X \sim P}[\phi(X)] - \mathbb{E}_{Y \sim Q}[\phi(Y)]\| \quad (2)$$

When the feature map corresponds to a characteristic kernel, such as the Gaussian kernel $k(x, y) = \exp(-\|x - y\|^2 / (2\sigma^2))$, MMD defines a metric over the space of probability distributions: it is non-negative, symmetric, satisfies the triangle inequality, and is zero if and only if the distributions are identical. The MMD can be computed using the “kernel trick” [37] with a positive definite kernel $k(x, y)$, allowing for implicit feature maps even in infinite-dimensional spaces.

While there are different ways of measuring distances between distributions, we chose MMD due to its desirable properties that allow us to obtain embeddings of the distributions in a computationally efficient manner. Notably, the MMD with a Gaussian kernel can be efficiently approximated using random Fourier features [34], providing a finite-dimensional embedding that preserves the geometry of the original kernel space.

3 Method

Our method, AutoQD, automatically discovers behavioral descriptors for quality-diversity optimization in sequential decision-making domains. The key insight is to use occupancy measures to characterize policy behaviors, and then extract low-dimensional behavioral descriptors that capture the main variations in policy behavior. The method operates in three main steps: (1) embedding policies into a high-dimensional space where distances approximate behavioral differences, (2) extracting low-dimensional behavioral descriptors from these embeddings, and (3) using these descriptors with standard QD algorithms to discover diverse, high-performing policies.

3.1 Policy embedding via random features

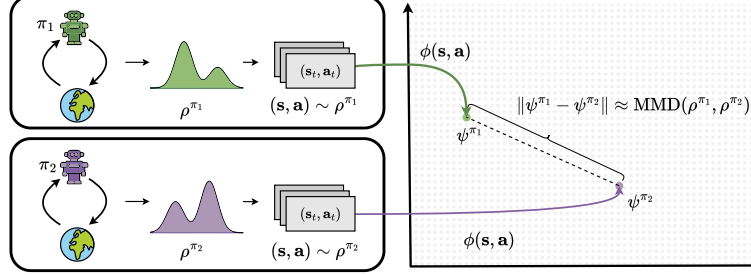


Figure 2: **Overview of the proposed policy embedding method.** Each policy π_i induces an occupancy measure ρ^{π_i} over state-action pairs. From sampled trajectories, a feature map ϕ embeds these policies into a finite-dimensional vector space. Theorem 1 guarantees that the Euclidean distance between embeddings approximates the Maximum Mean Discrepancy (MMD) between the corresponding occupancy measures.

To compare policy behaviors, we first embed policies into a finite-dimensional space whose Euclidean distances approximate the MMD between their occupancy measures. As established in Section 2, occupancy measures fully characterize policy behavior, and MMD with a Gaussian kernel provides a metric over them. However, the Gaussian kernel’s feature map is infinite-dimensional [37], and even though the kernel trick lets us compute pairwise MMDs from samples without explicitly computing the features [20], it only yields $\mathcal{O}(n^2)$ pairwise distances and no explicit embeddings. Therefore, we approximate the Gaussian kernel via random Fourier features [34] which lets us convert the infinite feature map into a D -dimensional mapping.

Given state $\mathbf{s} \in \mathcal{S}$ and action $\mathbf{a} \in \mathcal{A}$, we define a D -dimensional random feature map

$$\phi(\mathbf{s}, \mathbf{a}) = \sqrt{\frac{2}{D}} [\cos(\mathbf{w}_1^T [\mathbf{s}; \mathbf{a}] + \mathbf{b}_1), \dots, \cos(\mathbf{w}_D^T [\mathbf{s}; \mathbf{a}] + \mathbf{b}_D)] , \quad (3)$$

where $\mathbf{w}_i \sim \mathcal{N}(0, \sigma^{-2}I)$, $\mathbf{b}_i \sim \mathcal{U}(0, 2\pi)$, and $[\mathbf{s}; \mathbf{a}]$ denotes the concatenation of state and action vectors. The kernel width σ determines the scale at which state-action pairs are considered similar.

Consider a policy π with occupancy measure ρ^π . With a slight abuse of notation, let ϕ^π denote the embedding of π , defined as the empirical mean of the random Fourier features of n i.i.d. samples from ρ^π . That is, $\phi^\pi = \frac{1}{n} \sum_j \phi(\mathbf{s}_j^\pi, \mathbf{a}_j^\pi)$ where $(\mathbf{s}_1^\pi, \mathbf{a}_1^\pi), \dots, (\mathbf{s}_n^\pi, \mathbf{a}_n^\pi)$ are i.i.d. samples from ρ^π .

This embedding (which we refer to as *policy embedding*) approximates the expected feature map under the policy’s occupancy measure. The ℓ_2 distance between embeddings of two policies approximates their behavioral difference as measured by MMD of their occupancy measures:

$$\|\phi^{\pi_1} - \phi^{\pi_2}\| \approx \text{MMD}(\rho^{\pi_1}, \rho^{\pi_2}) \quad (4)$$

The quality of this approximation is characterized by the following theorem:

Theorem 1 (MMD Approximation). *For any two policies π_1, π_2 with occupancy measure ρ_1, ρ_2 and embeddings ϕ_1, ϕ_2 estimated by taking the mean of the D dimensional random Fourier features of n i.i.d. samples from each occupancy measure,*

$$\Pr \left[\left| \|\phi_1 - \phi_2\|_2 - \text{MMD}(\rho_1, \rho_2) \right| \geq \frac{3}{4}\varepsilon \right] \leq 2e^{-nc\varepsilon^2} + \mathcal{O} \left(\frac{1}{\varepsilon^2} \exp \left(\frac{-D\varepsilon^2}{64(d+2)} \right) \right) + 6e^{-\frac{n\varepsilon^2}{8}}, \quad (5)$$

where d is the dimension of state-action vectors and $c > 0$ is a constant.

A full proof is provided in Appendix A. This theorem shows that our embeddings can capture the geometry of the true occupancy measures, in the sense that, with high probability, the distances between the embeddings faithfully reflect the distances between the actual occupancy measures. By increasing the number of samples (n) and the number of random features (D), we can arbitrarily shrink the error.

We should also mention a subtlety regarding the practical computation of the policy embedding ϕ^π . To compute ϕ^π , we need i.i.d. samples from the occupancy measure ρ^π . We can obtain these by collecting n independent rollouts of π and selecting one state-action pair from each trajectory according to a Geometric distribution with parameter $1 - \gamma$. However, this leads to a very inefficient use of the collected data as it discards all but one transition from each trajectory. Therefore, in practice, we use ψ^π as defined in Eq. 6 instead of ϕ^π as the policy embedding. We motivate this by noting that ψ^π has the same expectation as ϕ^π but leverages all collected transitions, which potentially reduces the variance. Consequently, we use ψ^π to denote the policy embedding from this point on.

$$\psi^\pi = \frac{1}{n} \sum_{j=1}^n (1 - \gamma) \sum_{t=0}^T \gamma^t \phi(\mathbf{s}_t^j, \mathbf{a}_t^j) \quad (6)$$

3.2 The AutoQD algorithm

Given policy embeddings that encode behavioral differences, we project them into a low-dimensional space (with $k \ll D$ dimensions) and use them as behavioral descriptors (BDs) for QD optimization. As explained in Sec. 2.2, this is needed because QD algorithms discretize the behavior space along each dimension, resulting in an archive that grows exponentially with the dimension of BDs. We perform this using an affine transformation $\text{desc}(\pi) = \mathbf{A}\psi^\pi + \mathbf{b}$. The parameters of this transformation, $\mathbf{A} \in \mathbb{R}^{k \times D}$, $\mathbf{b} \in \mathbb{R}^k$, are derived by performing a modified version of PCA [17], which we call *Calibrated Weighted PCA* (*cwPCA*), on the embeddings of policies in the QD archive.

cwPCA makes minimal modification to PCA to better serve as a behavior descriptor for QD. Specifically, it applies PCA to policy embeddings *after weighting them by their fitness*, so that high-performing policies have greater influence on the principal directions. This biases the resulting components toward capturing behavior variation among strong policies, thereby encouraging exploration of diversity among high-quality behaviors. Following this, we apply a simple *calibration* step: we scale each output axis so that most projected embeddings lie in the range $[-1, 1]$. This ensures stable, fixed archive bounds throughout the algorithm. Full details including the precise form of the affine map and further motivation are provided in Appendix B.

Putting these pieces together, Algorithm 1 presents our method in its entirety. AutoQD combines the BDs described above with CMA-MAE to discover diverse and high-performing policies. It alternates

between two phases: (1) using the current behavioral descriptors to discover diverse policies with QD optimization, and (2) refining the behavioral descriptors based on the expanded archive of policies. For clarity and conciseness, Algorithm 1 abstracts the internal mechanics of CMA-MAE, omitting details of its initialization and update step. Detailed pseudocodes for these components are provided in Appendix C.

Algorithm 1 AutoQD

```

1: Input: MDP  $(\mathcal{S}, \mathcal{A}, P, R, \gamma)$ , embedding dimension  $D$ , behavioral descriptor dimension  $k$ , number of
   iterations  $n$ , Update schedule  $\{t_1, t_2, \dots\}$ 
2: Output: Archive of diverse and high-performing policies  $\mathbb{A}$ 
3: Initialize:
   CMA-MAE archive and parameters:  $\mathbb{A}, \text{QDState} \leftarrow \text{CMA\_MAE\_Init}(k)$ 
   Affine map parameters:  $\mathbf{A}, \mathbf{b}$ 
4: Sample random features  $\{\mathbf{w}_i\}_{i=1}^D \sim \mathcal{N}(0, \sigma^{-2}I)$  and offsets  $\{\mathbf{b}_i\}_{i=1}^D \sim \mathcal{U}(0, 2\pi)$ 
5: for  $t \in \{1, 2, \dots, n\}$  do
6:   if  $t \in \{t_1, t_2, \dots\}$  then ▷ Time to update descriptors
7:      $\Psi = [\psi^{\pi_1}, \dots, \psi^{\pi_m}]$  for  $\pi_i \in \mathbb{A}$  ▷ Policy embeddings as defined in Eq. 6
8:      $\mathbf{A}, \mathbf{b} \leftarrow \text{cwPCA}(\Psi, k)$ 
9:     Update behavioral descriptors:  $\text{desc}(\pi) = \mathbf{A}\psi^\pi + \mathbf{b}$ 
10:   end if
11:    $\mathbb{A}, \text{QDState} \leftarrow \text{CMA\_MAE\_Step}(\mathbb{A}, \text{QDState}, \text{desc})$  ▷ Perform one step of QD optimization
12: end for
13: return final archive  $\mathbb{A}$ 

```

4 Experiments

To empirically validate the effectiveness of AutoQD in discovering diverse and high-performing behaviors, we evaluated it on six standard continuous control tasks from the Gymnasium library [43], including five from the widely-used MuJoCo benchmark suite [42]. These environments are standard benchmarks for reinforcement learning methods and remain challenging for many evolutionary approaches, despite recent progress in the field.

4.1 Baselines

We compare our method to five baselines that have demonstrated strong performance in prior work and represent distinct strategies that have been employed to obtain diverse and high-quality populations.

RegularQD applies a standard QD algorithm using hand-crafted BDs specific to each environment. **Aurora** [7] learns a behavior space by training an autoencoder on the states observed by policies and uses the latent encoding of the last state in a rollout of the policy as its behavioral descriptor.

LSTM-Aurora [4] extends AURORA by using LSTMs to encode full trajectories and using the hidden state of the encoder LSTM as the behavioral descriptor.

DvD-ES [30] employs evolutionary strategies to jointly optimize a population of policies for both task performance and diversity.

SMERL [24] is an RL-based algorithm that trains a skill-conditioned policy using Soft Actor-Critic [22] and uses an additional reward derived from a discriminator to encourage diversity among skills.

All QD methods (AutoQD, RegularQD, Aurora, and LSTM-Aurora) use CMA-MAE [13] as the core optimization algorithm. Additionally, following [6], we use Toeplitz matrices to parameterize the policies for these methods to reduce the number of parameters and improve the performance of CMA-MAE. The full set of hyperparameters and more discussion about the implementation details are provided in Appendix D.

4.2 Evaluation metrics

Ensuring a fair comparison between algorithms that optimize different notions of diversity is inherently challenging. To address this, we employ three evaluation metrics: the Ground-Truth QD Score (GT QD Score), the Vendi Score (VS), and the Quality-Weighted Vendi Score (qVS).

Table 1: Comparison of AutoQD and baseline methods across six environments. Each environment is evaluated using GT QD Score (QD) reported in units of 10^4 for readability, qVS, and VS metrics. Reported values are the mean \pm standard error over evaluations with three different random seeds. Higher values indicate better performance for all metrics.

Metric	AutoQD	RegularQD	Aurora	LSTM-Aurora	DvD-ES	SMERL
Ant						
QD ($\times 10^4$)	361.43 \pm 2.17	182.58 \pm 2.53	5.57 \pm 1.48	19.24 \pm 1.1	0.29 \pm 0.1	1.02 \pm 0.23
qVS	60.23 \pm 9.4	39.35 \pm 3.99	0.56 \pm 0.01	1.11 \pm 0.41	0.49 \pm 0.00	0.97 \pm 0.15
VS	72.37 \pm 10.63	39.49 \pm 3.93	1.11 \pm 0.01	1.9 \pm 0.54	1.00 \pm 0.00	1.29 \pm 0.18
HalfCheetah						
QD ($\times 10^4$)	30.78 \pm 2.72	24.91 \pm 3.43	11.35 \pm 4.69	11.38 \pm 2.02	0.85 \pm 0.23	1.61 \pm 0.37
qVS	1.35 \pm 0.6	2.07 \pm 0.13	2.39 \pm 0.42	1.71 \pm 0.21	1.15 \pm 0.09	1.78 \pm 0.51
VS	5.29 \pm 1.59	3.44 \pm 0.34	5.8 \pm 0.81	4.83 \pm 0.16	1.19 \pm 0.11	3.55 \pm 0.56
Hopper						
QD ($\times 10^4$)	1.84 \pm 0.29	1.2 \pm 0.03	1.06 \pm 0.09	1.36 \pm 0.01	0.56 \pm 0.18	0.97 \pm 0.15
qVS	1.94 \pm 0.04	1.35 \pm 0.05	0.66 \pm 0.09	0.36 \pm 0.08	0.9 \pm 0.32	1.81 \pm 0.22
VS	4.5 \pm 0.2	2.85 \pm 0.04	2.67 \pm 0.09	2.13 \pm 0.29	1.27 \pm 0.13	3.34 \pm 0.24
Swimmer						
QD ($\times 10^4$)	21.31 \pm 4.57	11.09 \pm 0.08	8.05 \pm 0.58	10.26 \pm 0.72	0.22 \pm 0.02	0.02 \pm 0.00
qVS	6.04 \pm 0.66	3.17 \pm 0.19	3.09 \pm 0.15	3.82 \pm 0.77	1.16 \pm 0.1	0.24 \pm 0.06
VS	16.92 \pm 3.68	4.67 \pm 0.35	6.75 \pm 0.25	7.21 \pm 1.95	1.2 \pm 0.13	2.16 \pm 0.57
Walker2d						
QD ($\times 10^4$)	18.36 \pm 2.58	11.39 \pm 0.55	7.71 \pm 1.26	12.99 \pm 0.77	0.61 \pm 0.11	1.17 \pm 0.14
qVS	7.22 \pm 2.08	9.08 \pm 0.53	1.11 \pm 0.08	2.12 \pm 0.07	1.47 \pm 0.26	2.74 \pm 0.42
VS	8.4 \pm 3.2	10.17 \pm 0.89	2.5 \pm 0.13	4.17 \pm 0.47	1.58 \pm 0.29	3.2 \pm 0.17
BipedalWalker						
QD ($\times 10^4$)	6.09 \pm 0.22	1.81 \pm 0.02	3.0 \pm 0.2	3.36 \pm 0.08	0.09 \pm 0.03	0.14 \pm 0.01
qVS	5.16 \pm 0.17	0.81 \pm 0.02	1.12 \pm 0.08	1.67 \pm 0.34	1.03 \pm 0.02	2.11 \pm 0.27
VS	12.17 \pm 0.52	1.57 \pm 0.03	2.88 \pm 0.21	3.36 \pm 0.46	1.06 \pm 0.00	5.54 \pm 0.42

The **GT QD Score** is the QD score of a population when its solutions are inserted into an archive that uses hand-designed behavioral descriptors. It evaluates the quality and diversity of a population using expert-defined behavior spaces. We note that these BDs are commonly used in prior work and are the same ones that the RegularQD baseline uses.

To evaluate diversity in a method-agnostic way, we use the **Vendi Score (VS)** [16]. This metric quantifies a population’s diversity based on pairwise similarities, without relying on hand-designed descriptors. Given a population of size n and a positive-definite kernel matrix $K \in \mathbb{R}^{n \times n}$ where $K_{ij} \in [0, 1]$ is the similarity of the i -th and j -th members of the population, the Vendi Score is defined as $VS(K) = \exp\left(-\sum_{i=1}^n \bar{\lambda}_i \log \bar{\lambda}_i\right)$, where $\bar{\lambda}_1, \bar{\lambda}_2, \dots, \bar{\lambda}_n$ are the normalized eigenvalues of K (i.e., they sum to one). Conceptually, the VS measures the *effective population size*, serving as a measure of population diversity.

The **Quality-Weighted Vendi Score (qVS)** [26] extends the VS by incorporating solution quality: $qVS(K) = \left(\frac{1}{n} \sum_{i=1}^n J(\pi_i)\right) VS(K)$, where $J(\pi_i)$ is the fitness of the i -th individual, π_i . Notably, qVS requires all objectives to be positive. To accommodate this, we add a constant offset to all objectives in each environment. We then scale them to the $[0, 1]$ range by dividing each return by the highest mean return achieved by any of the algorithms in that environment, prior to computing qVS.

To construct the kernel matrix K used by VS and qVS, we use a Gaussian kernel applied to the inner product of the Random Fourier Feature (RFF) embeddings of policies. Although these embeddings are structurally similar to those used by AutoQD, we employ a separate, larger set of RFFs solely for evaluation to ensure a fair comparison. Our choice of embeddings is motivated by our theoretical results showing that distances between these embeddings asymptotically reflect distances between policy occupancy measures. For a more detailed analysis of qVS and its theoretical properties, we refer the reader to [26].

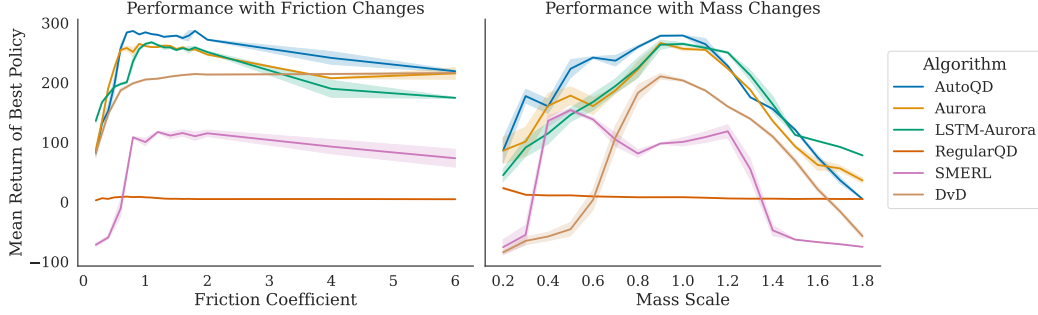


Figure 3: Performance of the best policy found by each algorithm under changing friction (left) or mass scale (right). The shaded regions represent the standard error across 32 evaluation seeds.

Metric	AutoQD	RegularQD	Aurora	LSTM-Aurora	DvD-ES	SMERL
Friction AUC	1429.66	30.27	1309.41	1226.29	1204.03	496.23
Mass AUC	295.65	12.8	260.60	271.83	113.68	71.38

Table 2: Comparison of Area Under the Curve (AUC) for each algorithm across friction and mass variations. Higher values indicate better adaptability to changing parameters.

4.3 Main results: policy discovery

Table 1 compares AutoQD with the baseline algorithms across six environments. For each algorithm-environment pair, we report the mean and standard error across three random seeds. As shown in the table, our method consistently outperforms the baselines in most environments; The only exceptions being the **Walker2d** and **HalfCheetah** environments, where the best qVS and VS are achieved by RegularQD and Aurora, respectively.

In HalfCheetah, AutoQD was able to discover diverse policies, but the policies tended to be relatively low performing, a sentiment that is reflected by its high VS and low qVS. Upon visual inspection, we noticed that AutoQD discovered many policies that moved forward by “sliding” through subtle joint movements. While these behaviors were diverse and novel, they generally resulted in slow movement, and as a result, lower overall rewards. Furthermore, in Walker2d, AutoQD seemingly overemphasized the role of the bottom-most (feet) joints, missing out on interesting behavioral variations that could be achieved, for instance, by fully lifting the legs. Despite this, AutoQD ranked second in this domain, outperforming all other baselines by a significant margin.

4.4 Application: adaptation to different dynamics

A key motivation for discovering diverse populations is the ability to adapt to changes in environment dynamics. A collection of behaviorally diverse policies is more likely to include some policy that maintains a high performance under altered conditions. To investigate this, we evaluated the populations produced by AutoQD and the baselines in environments with modified dynamics.

Specifically, we used the BipedalWalker environment and introduced two types of variations: scaling the friction coefficient and altering the mass of the robot. Figure 3 shows the performance of the best policy found by each method under modified dynamics. The area under these curves (AUC) provides a scalar measure of robustness: higher AUC indicates greater adaptability to environmental changes. Table 2 summarizes these AUC comparisons. As can be seen, the collection of policies found by AutoQD maintains a relatively high performance in the face of both types of variations, outperforming the other baselines in terms of AUC.

5 Related work

Quality-Diversity methods. Quality-Diversity optimization algorithms discover collections of solutions that balance performance and diversity across specified behavioral dimensions [32]. MAP-Elites [9] pioneered this approach by maintaining an archive of solutions organized by their behavioral characteristics. CMA-ME [14] reformulated the QD problem as single objective optimization, enabling the use of powerful blackbox optimization methods like CMA-ES [23] instead of relying solely on random mutations. The more recent CMA-MAE [13], which is used as the backbone QD algorithm in this paper, further improved this method by introducing the idea of *soft archives*. More recently, gradient-based variants like DQD [12], PGA-MAP-Elites [27] and PPGA [1] have made further progress by leveraging policy gradients.

Unsupervised QD approaches. Most prior work such as Aurora [7], LSTM-Aurora [4], and TAXONS [29] learn behavioral descriptors by training autoencoders on states, relying on the hypothesis that representations capturing state information also reflect policy behavior. [21] argues in favor of this approach by showing that the entropy of the encoded trajectories lower-bounds the entropy of the full trajectories. However, their analysis assumes a discrete state space and does not formally link trajectory entropy to policy diversity. In contrast, AutoQD constructs embeddings based on policy-induced occupancy measures via Random Fourier Features, offering a principled and theoretically grounded representation of behavior.

Unsupervised RL for skill discovery. The RL community has explored related approaches for learning diverse behaviors. DIAYN [11] maximizes mutual information between skills and states, encouraging skills to visit distinct regions of the state space without using reward signals. DADS [38] extends this by maximizing mutual information between skills and transitions, favoring predictable outcomes. However, both methods ignore the task reward. SMERL [24] and DoMiNo [44] incorporate task rewards into diversity objectives. SMERL directly augments DIAYN’s objective with task rewards, while DoMiNo frames the problem as a constrained MDP, maximizing diversity by encouraging distance between state occupancies of near-optimal policies. Both highlight the benefits of diverse, high-performing policies but require a fixed number of skills and tend to scale poorly with skill count.

Policy embedding and representation. In a middle ground between QD methods and unsupervised RL approaches, DvD [30] characterizes policies through their actions in (random) set of states, resembling the off-policy embeddings from [28]. However, these embeddings lack the theoretical backing that our method provides. Furthermore, like SMERL, their proposed algorithm requires specifying the number of policies in advance and faces stability issues as this number increases. [5] also share conceptual similarities with our approach, though in the context of transfer learning and generalization. They learn a Q-function basis by training policies on features from randomly initialized networks. In contrast, we use random Fourier features to embed occupancy measures directly, enabling QD optimization without prior RL training. Our use of Random Fourier Features [34] to embed occupancy measures connects to theoretical work on kernel approximations [36, 35]. A key insight of our approach is recognizing that these techniques can be applied to represent policy behaviors in a theoretically principled way. By embedding occupancy measures and applying dimensionality reduction, we automatically generate behavioral descriptors that capture essential policy characteristics without manual specification.

6 Limitations and future work

We introduced **AutoQD**, a novel approach for applying Quality-Diversity (QD) optimization to sequential decision-making tasks without handcrafted behavioral descriptors. By embedding policies based on their occupancy measures and projecting to a compact descriptor space, AutoQD enables integration with standard QD algorithms and achieves strong empirical performance.

Limitations. AutoQD has several limitations. First, the choice of kernel bandwidth affects the sensitivity of the embeddings. While we use a fixed bandwidth in this work, dynamically adapting it during training could allow the embeddings to better capture behavioral distinctions at different stages of learning. Second, in highly stochastic environments, accurately estimating policy embeddings may

require a large number of trajectories, which can impact sample efficiency. Additionally, AutoQD inherits limitations from the underlying QD algorithms it relies on. Existing QD methods often struggle to scale with larger policy networks or high-dimensional behavior representations due to their reliance on discretized behavior archives [40]. While this is not a fundamental limitation of our method, it constrains its practical scalability within current QD frameworks. Furthermore, although QD methods promote behavioral diversity, the performance of the best policy discovered may fall short of that achieved by reinforcement learning methods optimized solely for reward.

Future Work. Future directions include integrating AutoQD with gradient-based QD methods to improve sample efficiency and extending the approach to environments with image-based observations. Additionally, the policy embeddings produced by AutoQD could find applications beyond QD, including open-ended learning, imitation learning, and inverse reinforcement learning. They may also prove useful for analyzing learned policies, for example through clustering and other forms of characterization.

References

- [1] Sumeet Batra, Bryon Tjanaka, Matthew Christopher Fontaine, Aleksei Petrenko, Stefanos Nikolaidis, and Gaurav S. Sukhatme. Proximal policy gradient arborescence for quality diversity reinforcement learning. In *The Twelfth International Conference on Learning Representations, ICLR 2024, Vienna, Austria, May 7-11, 2024*. OpenReview.net, 2024. URL <https://openreview.net/forum?id=TFKIfhvdMz>.
- [2] Varun Bhatt, Bryon Tjanaka, Matthew Fontaine, and Stefanos Nikolaidis. Deep surrogate assisted generation of environments. *Advances in Neural Information Processing Systems*, 35: 37762–37777, 2022. URL http://papers.nips.cc/paper_files/paper/2022/hash/f649556471416b35e60ae0de7c1e3619-Abstract-Conference.html.
- [3] Raphaël Boige, Guillaume Richard, Jérémie Dona, Thomas Pierrot, and Antoine Cully. Gradient-informed quality diversity for the illumination of discrete spaces. In *Proceedings of the Genetic and Evolutionary Computation Conference*, pages 119–128, 2023.
- [4] Félix Chalumeau, Raphaël Boige, Bryan Lim, Valentin Macé, Maxime Allard, Arthur Flajolet, Antoine Cully, and Thomas Pierrot. Neuroevolution is a competitive alternative to reinforcement learning for skill discovery. In *The Eleventh International Conference on Learning Representations, ICLR, 2023*. URL <https://openreview.net/forum?id=6BH1ZgyPOZY>.
- [5] Boyuan Chen, Chuning Zhu, Pulkit Agrawal, Kaiqing Zhang, and Abhishek Gupta. Self-supervised reinforcement learning that transfers using random features. *Advances in Neural Information Processing Systems*, 36:56411–56436, 2023.
- [6] Krzysztof Choromanski, Mark Rowland, Vikas Sindhwani, Richard Turner, and Adrian Weller. Structured evolution with compact architectures for scalable policy optimization. In *International Conference on Machine Learning*, pages 970–978. PMLR, 2018.
- [7] Antoine Cully. Autonomous skill discovery with quality-diversity and unsupervised descriptors. In *Proceedings of the Genetic and Evolutionary Computation Conference*, pages 81–89, 2019.
- [8] Antoine Cully, Jeff Clune, Danesh Tarapore, and Jean-Baptiste Mouret. Robots that can adapt like animals. *Nature*, 521(7553):503–507, 2015.
- [9] Antoine Cully, Jeff Clune, Danesh Tarapore, and Jean-Baptiste Mouret. Robots that can adapt like animals. *Nature*, 521(7553):503–507, 2015.
- [10] Miguel Duarte, Jorge Gomes, Sancho Moura Oliveira, and Anders Lyhne Christensen. Evolution of repertoire-based control for robots with complex locomotor systems. *IEEE Transactions on Evolutionary Computation*, 22(2):314–328, 2017.
- [11] Benjamin Eysenbach, Abhishek Gupta, Julian Ibarz, and Sergey Levine. Diversity is all you need: Learning skills without a reward function. In *7th International Conference on Learning Representations, ICLR, 2019*. URL <https://openreview.net/forum?id=SJx63jRqFm>.

- [12] Matthew Fontaine and Stefanos Nikolaidis. Differentiable quality diversity. *Advances in Neural Information Processing Systems*, 34:10040–10052, 2021.
- [13] Matthew Fontaine and Stefanos Nikolaidis. Covariance matrix adaptation map-annealing. In *Proceedings of the genetic and evolutionary computation conference*, pages 456–465, 2023.
- [14] Matthew C Fontaine, Julian Togelius, Stefanos Nikolaidis, and Amy K Hoover. Covariance matrix adaptation for the rapid illumination of behavior space. In *Proceedings of the 2020 genetic and evolutionary computation conference*, pages 94–102, 2020.
- [15] Matthew C Fontaine, Ruilin Liu, Ahmed Khalifa, Jignesh Modi, Julian Togelius, Amy K Hoover, and Stefanos Nikolaidis. Illuminating mario scenes in the latent space of a generative adversarial network. In *Proceedings of the AAAI Conference on Artificial Intelligence*, volume 35, pages 5922–5930, 2021.
- [16] Dan Friedman and Adji Bousso Dieng. The vendi score: A diversity evaluation metric for machine learning. *Trans. Mach. Learn. Res.*, 2023. URL <https://openreview.net/forum?id=g970HbQyk1>.
- [17] Karl Pearson F.R.S. Liii. on lines and planes of closest fit to systems of points in space. *The London, Edinburgh, and Dublin Philosophical Magazine and Journal of Science*, 2(11):559–572, 1901. doi: 10.1080/14786440109462720.
- [18] Damien Garreau, Wittawat Jitkittum, and Motonobu Kanagawa. Large sample analysis of the median heuristic. *arXiv preprint arXiv:1707.07269*, 2017.
- [19] Daniele Gravina, Ahmed Khalifa, Antonios Liapis, Julian Togelius, and Georgios N Yannakakis. Procedural content generation through quality diversity. In *2019 IEEE Conference on Games (CoG)*, pages 1–8. IEEE, 2019.
- [20] Arthur Gretton, Karsten M Borgwardt, Malte J Rasch, Bernhard Schölkopf, and Alexander Smola. A kernel two-sample test. *The Journal of Machine Learning Research*, 13(1):723–773, 2012.
- [21] Luca Grillotti and Antoine Cully. Discovering unsupervised behaviours from full state trajectories. In *ICLR Workshop on Agent Learning in Open-Endedness*.
- [22] Tuomas Haarnoja, Aurick Zhou, Pieter Abbeel, and Sergey Levine. Soft actor-critic: Off-policy maximum entropy deep reinforcement learning with a stochastic actor. In *International conference on machine learning*, pages 1861–1870. Pmlr, 2018.
- [23] Nikolaus Hansen. The cma evolution strategy: A tutorial. *arXiv preprint arXiv:1604.00772*, 2016.
- [24] Saurabh Kumar, Aviral Kumar, Sergey Levine, and Chelsea Finn. One solution is not all you need: Few-shot extrapolation via structured maxent rl. *Advances in Neural Information Processing Systems*, 33:8198–8210, 2020.
- [25] Joel Lehman and Kenneth O Stanley. Abandoning objectives: Evolution through the search for novelty alone. *Evolutionary computation*, 19(2):189–223, 2011.
- [26] Quan Nguyen and Adji Bousso Dieng. Quality-weighted vendi scores and their application to diverse experimental design. In *Forty-first International Conference on Machine Learning, ICML 2024, Vienna, Austria, July 21-27, 2024*. URL <https://openreview.net/forum?id=gbd9MAc9p0>.
- [27] Olle Nilsson and Antoine Cully. Policy gradient assisted map-elites. In *Proceedings of the Genetic and Evolutionary Computation Conference*, pages 866–875, 2021.
- [28] Aldo Pacchiano, Jack Parker-Holder, Yunhao Tang, Krzysztof Choromanski, Anna Choromanska, and Michael Jordan. Learning to score behaviors for guided policy optimization. In *International Conference on Machine Learning*, pages 7445–7454. PMLR, 2020.

- [29] Giuseppe Paolo, Alban Laflaquiere, Alexandre Coninx, and Stephane Doncieux. Unsupervised learning and exploration of reachable outcome space. In *2020 IEEE International Conference on Robotics and Automation (ICRA)*, pages 2379–2385. IEEE, 2020.
- [30] Jack Parker-Holder, Aldo Pacchiano, Krzysztof M Choromanski, and Stephen J Roberts. Effective diversity in population based reinforcement learning. *Advances in Neural Information Processing Systems*, 33:18050–18062, 2020.
- [31] Thomas Pierrot, Valentin Macé, Felix Chalumeau, Arthur Flajolet, Geoffrey Cideron, Karim Beguir, Antoine Cully, Olivier Sigaud, and Nicolas Perrin-Gilbert. Diversity policy gradient for sample efficient quality-diversity optimization. In *Proceedings of the Genetic and Evolutionary Computation Conference*, pages 1075–1083, 2022.
- [32] Justin K Pugh, Lisa B Soros, and Kenneth O Stanley. Quality diversity: A new frontier for evolutionary computation. *Frontiers in Robotics and AI*, 3:40, 2016.
- [33] Martin L Puterman. *Markov decision processes: discrete stochastic dynamic programming*. John Wiley & Sons, 2014.
- [34] Ali Rahimi and Benjamin Recht. Random features for large-scale kernel machines. *Advances in neural information processing systems*, 20, 2007.
- [35] Ali Rahimi and Benjamin Recht. Weighted sums of random kitchen sinks: Replacing minimization with randomization in learning. *Advances in neural information processing systems*, 21, 2008.
- [36] Alessandro Rudi and Lorenzo Rosasco. Generalization properties of learning with random features. *Advances in neural information processing systems*, 30, 2017.
- [37] Bernhard Schölkopf and Alexander J Smola. *Learning with kernels: support vector machines, regularization, optimization, and beyond*. MIT press, 2002.
- [38] Archit Sharma, Shixiang Gu, Sergey Levine, Vikash Kumar, and Karol Hausman. Dynamics-aware unsupervised discovery of skills. In *8th International Conference on Learning Representations, ICLR*, 2020. URL <https://openreview.net/forum?id=HJgLZR4KvH>.
- [39] Bryon Tjanaka, Matthew C Fontaine, Julian Togelius, and Stefanos Nikolaidis. Approximating gradients for differentiable quality diversity in reinforcement learning. In *Proceedings of the Genetic and Evolutionary Computation Conference*, pages 1102–1111, 2022.
- [40] Bryon Tjanaka, Matthew C Fontaine, David H Lee, Aniruddha Kalkar, and Stefanos Nikolaidis. Training diverse high-dimensional controllers by scaling covariance matrix adaptation map-annealing. *IEEE Robotics and Automation Letters*, 8(10):6771–6778, 2023.
- [41] Bryon Tjanaka, Matthew C Fontaine, David H Lee, Yulun Zhang, Nivedit Reddy Balam, Nathaniel Dennler, Sujay S Garlanka, Nikitas Dimitri Klapsis, and Stefanos Nikolaidis. Pyribs: A bare-bones python library for quality diversity optimization. In *Proceedings of the Genetic and Evolutionary Computation Conference, GECCO ’23*, page 220–229, New York, NY, USA, 2023. Association for Computing Machinery. ISBN 9798400701191. doi: 10.1145/3583131.3590374. URL <https://doi.org/10.1145/3583131.3590374>.
- [42] Emanuel Todorov, Tom Erez, and Yuval Tassa. Mujoco: A physics engine for model-based control. In *2012 IEEE/RSJ international conference on intelligent robots and systems*, pages 5026–5033. IEEE, 2012.
- [43] Mark Towers, Ariel Kwiatkowski, Jordan Terry, John U Balis, Gianluca De Cola, Tristan Deleu, Manuel Goulao, Andreas Kallinteris, Markus Krimmel, Arjun KG, et al. Gymnasium: A standard interface for reinforcement learning environments. *arXiv preprint arXiv:2407.17032*, 2024.
- [44] Tom Zahavy, Yannick Schroecker, Feryal M. P. Behbahani, Kate Baumli, Sebastian Flennerhag, Shaobo Hou, and Satinder Singh. Discovering policies with domino: Diversity optimization maintaining near optimality. In *The Eleventh International Conference on Learning Representations, ICLR*, 2023. URL <https://openreview.net/forum?id=kjkdzBW3b8p>.

A Proof of Theorem 1

As our main result, we show that the ℓ_2 distance between our embeddings of occupancy measures (estimated from samples) is a good approximation of the true MMD between occupancy measures. Formally, let P and Q be two occupancy measures defined over d dimensional state-action vectors. Let k be the Gaussian kernel and $\phi : \mathbb{R}^d \rightarrow \mathbb{R}^D$ be the random Fourier features that map state-action vectors to a D dimensional embedding space. Given n samples $\{x_1, \dots, x_n\}$ from P we define $\phi_P = \frac{1}{n} \sum_i \phi(x_i)$ as the embedding of P . Similarly, we define ϕ_Q as the embedding of Q obtained from n samples y_1, \dots, y_n . The claim is that $\|\phi_P - \phi_Q\|_2$ is a good approximation of $\text{MMD}(P, Q)$. The following are the steps we take to complete the proof.

1. We start by showing that with high probability $\text{MMD}^2(P, Q)$ and $\|\phi_P - \phi_Q\|_2^2$ are close to one another. This is done in four steps where we
 - (a) show that $\|\phi_P - \phi_Q\|_2^2$ is close to $\widetilde{\text{MMD}}$,
 - (b) show that $\widetilde{\text{MMD}}$ is close to $\widehat{\text{MMD}}$,
 - (c) show that $\widehat{\text{MMD}}$ is close to MMD^2 ,
 - (d) conjoin the previous three bounds to show that $\|\phi_P - \phi_Q\|_2^2$ is close to MMD^2 .
2. Then, we show that $\text{MMD}(P, Q)$ is close to $\|\phi_P - \phi_Q\|_2$.

Recall that from the definition of MMD and using the kernel trick we have

$$\text{MMD}^2(P, Q) = \mathbb{E}_{X, X' \sim P}[k(X, X')] + \mathbb{E}_{Y, Y' \sim Q}[k(Y, Y')] - 2\mathbb{E}_{X \sim P, Y \sim Q}[k(X, Y)]. \quad (7)$$

Let us start from $\|\phi_P - \phi_Q\|_2^2$ and step-by-step get closer to the quantity above. We have

$$\|\phi_P - \phi_Q\|_2^2 = (\phi_P - \phi_Q)^T (\phi_P - \phi_Q) \quad (8)$$

$$= \phi_P^T \phi_P + \phi_Q^T \phi_Q - 2\phi_P^T \phi_Q. \quad (9)$$

Examining each of these three terms more carefully, we see that

$$\phi_P^T \phi_P = \frac{1}{n^2} \sum_{i,j} \phi(x_i)^T \phi(x_j) = \frac{1}{n^2} \sum_i \phi(x_i)^T \phi(x_i) + \frac{1}{n^2} \sum_{i \neq j} \phi(x_i)^T \phi(x_j), \quad (10)$$

$$\phi_Q^T \phi_Q = \frac{1}{n^2} \sum_{i,j} \phi(y_i)^T \phi(y_j) = \frac{1}{n^2} \sum_i \phi(y_i)^T \phi(y_i) + \frac{1}{n^2} \sum_{i \neq j} \phi(y_i)^T \phi(y_j), \quad (11)$$

$$\phi_P^T \phi_Q = \frac{1}{n^2} \sum_{i,j} \phi(x_i)^T \phi(y_j). \quad (12)$$

Now, let $\widetilde{\text{MMD}}$ be defined as

$$\widetilde{\text{MMD}} = \frac{1}{n} \sum_{i=1}^n \phi(x_i)^T \phi(x'_i) + \frac{1}{n} \sum_{i=1}^n \phi(y_i)^T \phi(y'_i) - \frac{2}{n} \sum_{i=1}^n \phi(x_i)^T \phi(y_i), \quad (13)$$

where x_i, x'_i 's are i.i.d. samples from P and y_i, y'_i are i.i.d. samples from Q . From this, we can see that the expectations of $\|\phi_P - \phi_Q\|_2^2$ and $\widetilde{\text{MMD}}$ are quite similar and in fact, they are the same at the limit of $n \rightarrow \infty$.

$$\mathbb{E} [\|\phi_P - \phi_Q\|_2^2] = \left(\frac{n-1}{n} \right) \mathbb{E} [\widetilde{\text{MMD}}] + \frac{1}{n} \mathbb{E}_{X \sim P, Y \sim Q} [\|\phi(X)\|^2 + \|\phi(Y)\|^2]. \quad (14)$$

Using the fact that, by the definition of random Fourier features, the entries of $\phi(x)$ are bounded in $[-\frac{1}{\sqrt{D}}, \frac{1}{\sqrt{D}}]$ we see that the difference between $\mathbb{E} [\|\phi_P - \phi_Q\|_2^2]$ and $\mathbb{E} [\widetilde{\text{MMD}}]$ is at most $\mathcal{O}(\frac{1}{n})$.

Now, by applying Hoeffding's inequality to bound the deviation of each of these from their respective means we get that with probability at least $1 - \delta$

$$|\|\phi_P - \phi_Q\|^2 - \mathbb{E} [\|\phi_P - \phi_Q\|^2]| \leq \sqrt{\frac{\log \frac{2}{\delta}}{2n}}, \quad (15)$$

and similarly with probability at least $1 - \delta$

$$|\widetilde{\text{MMD}} - \mathbb{E} [\widetilde{\text{MMD}}]| \leq \sqrt{\frac{\log \frac{2}{\delta}}{2n}}. \quad (16)$$

Combining these with the triangle inequality and using the union bound we get that with probability at least $1 - 2\delta$

$$|\|\phi_P - \phi_Q\|^2 - \widetilde{\text{MMD}}| \leq 2\sqrt{\frac{\log \frac{2}{\delta}}{2n}} + \mathcal{O}\left(\frac{1}{n}\right). \quad (17)$$

For large values of n the first term on the right hand side dominates, therefore we can say that with probability at least $1 - 2\delta$

$$\left| \|\phi_P - \phi_Q\|^2 - \widetilde{\text{MMD}} \right| = \mathcal{O} \left(\sqrt{\frac{-\log \delta}{n}} \right). \quad (18)$$

Therefore, for some non-negative constant c we have

$$\Pr \left[\left| \|\phi_P - \phi_Q\|^2 - \widetilde{\text{MMD}} \right| \geq \varepsilon \right] \leq 2e^{-nc\varepsilon^2} \quad (19)$$

We now move on to the next part of the proof. Define $\widehat{\text{MMD}}$ as follows.

$$\widehat{\text{MMD}} = \frac{1}{n} \sum_{i=1}^n k(x_i, x'_i) + \frac{1}{n} \sum_{i=1}^n k(y_i, y'_i) - \frac{2}{n} \sum_{i=1}^n k(x_i, y_i). \quad (20)$$

In words, $\widehat{\text{MMD}}$ is just like $\widetilde{\text{MMD}}$ but with all of the inner products of random Fourier features replaced by kernel operations. We can see that

$$|\widehat{\text{MMD}} - \widetilde{\text{MMD}}| = \left| \frac{1}{n} \sum_{i=1}^n [k(x_i, x'_i) - \phi(x_i)^T \phi(x'_i)] \right| \quad (21)$$

$$+ \frac{1}{n} \sum_{i=1}^n [k(y_i, y'_i) - \phi(y_i)^T \phi(y'_i)] \quad (22)$$

$$- \frac{2}{n} \sum_{i=1}^n [k(x_i, y_i) - \phi(x_i)^T \phi(y_i)] \Big|. \quad (23)$$

Next, we make use of the following lemma that guarantees the uniform convergence of Fourier features stated in section 3 of [34]:

$$\Pr \left[\sup_{x, y} |\phi(x)^T \phi(y) - k(x, y)| \geq \varepsilon \right] \leq \mathcal{O} \left(\frac{1}{\varepsilon^2} \exp \left(-\frac{D\varepsilon^2}{4(d+2)} \right) \right) \quad (24)$$

where d is the dimensionality of the state-action vectors. This implies that each of the terms (summands) in 23 is at most $\frac{\varepsilon}{4}$ with probability at least $1 - \mathcal{O} \left(\frac{16}{\varepsilon^2} \exp \left(-\frac{D\varepsilon^2}{64(d+2)} \right) \right)$. Substituting $\frac{\varepsilon}{4}$ in 23 and using the triangle inequality, we see that

$$|\widehat{\text{MMD}} - \widetilde{\text{MMD}}| \leq \frac{1}{n} \sum_{i=1}^n \frac{\varepsilon}{4} + \frac{1}{n} \sum_{i=1}^n \frac{\varepsilon}{4} + \frac{2}{n} \sum_{i=1}^n \frac{\varepsilon}{4} = \varepsilon, \quad (25)$$

with probability at least $1 - \mathcal{O}\left(\frac{16}{\varepsilon^2} \exp\left(-\frac{D\varepsilon^2}{64(d+2)}\right)\right)$. Therefore,

$$\Pr\left[|\widehat{\text{MMD}} - \widetilde{\text{MMD}}| \geq \varepsilon\right] \leq \mathcal{O}\left(\frac{16}{\varepsilon^2} \exp\left(\frac{-D\varepsilon^2}{64(d+2)}\right)\right). \quad (26)$$

This brings us to the third step of the proof where we connect $\widehat{\text{MMD}}$ with $\text{MMD}^2(P, Q)$. This is more straight forward to show, since each term in the former is the Monte Carlo estimate of the corresponding expectation in the latter. More formally,

$$\widehat{\text{MMD}} - \text{MMD}^2(P, Q) = \left(\frac{1}{n} \sum_{i=1}^n k(x_i, x'_i) - \mathbb{E}_P[k(X, X')]\right) \quad (27)$$

$$+ \left(\frac{1}{n} \sum_{i=1}^n k(y_i, y'_i) - \mathbb{E}_Q[k(Y, Y')]\right) \quad (28)$$

$$- 2 \left(\frac{1}{n} \sum_{i=1}^n k(x_i, y_i) - \mathbb{E}_{P,Q}[k(X, Y)]\right). \quad (29)$$

Now note that in each of the three parentheses the first term is the empirical mean and the second term is the true mean. Combining this with the fact that $k(x, y)$ is always between 0 and 1, we can apply Hoeffding's inequality to each term to get a tail bound for each of them. For example, for the first parenthesis we get

$$\Pr\left(\left|\frac{1}{n} \sum_{i=1}^n k(x_i, x'_i) - \mathbb{E}_P[k(X, X')]\right| \geq \frac{\varepsilon}{4}\right) \leq 2 \exp \frac{-n\varepsilon^2}{8}. \quad (30)$$

Applying the triangle inequality and the union bound we get

$$\Pr\left[|\widehat{\text{MMD}} - \text{MMD}^2(P, Q)| \geq \varepsilon\right] \leq 6 \exp \frac{-n\varepsilon^2}{8} \quad (31)$$

Now, we can combine 19, 26, and 31 to bound the difference between $\|\phi_P - \phi_Q\|_2^2$ and $\text{MMD}^2(P, Q)$. Note that by triangle inequality

$$|\|\phi_P - \phi_Q\|_2^2 - \text{MMD}^2(P, Q)| \leq |\|\phi_P - \phi_Q\|_2^2 - \widetilde{\text{MMD}}| + |\widetilde{\text{MMD}} - \widehat{\text{MMD}}| + |\widehat{\text{MMD}} - \text{MMD}^2|. \quad (32)$$

Combining the bounds that we have for each of the terms on the right hand side, we get

$$\Pr\left[|\|\phi_P - \phi_Q\|_2^2 - \text{MMD}^2(P, Q)| \geq 3\varepsilon\right] \leq 2e^{-nc\varepsilon^2} + \mathcal{O}\left(\frac{1}{\varepsilon^2} \exp\left(\frac{-D\varepsilon^2}{64(d+2)}\right)\right) + 6e^{-\frac{n\varepsilon^2}{8}}. \quad (33)$$

This ensures that as we increase the number of samples n and the number of features D , the probability of error decays exponentially.

Lastly, we shall derive a bound on $|\|\phi_P - \phi_Q\|_2 - \text{MMD}(P, Q)|$. Note that

$$|\|\phi_P - \phi_Q\|_2^2 - \text{MMD}^2(P, Q)| = |\|\phi_P - \phi_Q\|_2 - \text{MMD}(P, Q)| (\|\phi_P - \phi_Q\|_2 + \text{MMD}(P, Q)) \quad (34)$$

$$\leq |\|\phi_P - \phi_Q\|_2 - \text{MMD}(P, Q)|(2 + 2) \quad (35)$$

$$\leq 4|\|\phi_P - \phi_Q\|_2 - \text{MMD}(P, Q)|. \quad (36)$$

Replacing this back into the bound in 33 we get

$$\Pr\left[|\|\phi_P - \phi_Q\|_2 - \text{MMD}(P, Q)| \geq \frac{3}{4}\varepsilon\right] \leq 2e^{-nc\varepsilon^2} + \mathcal{O}\left(\frac{1}{\varepsilon^2} \exp\left(\frac{-D\varepsilon^2}{64(d+2)}\right)\right) + 6e^{-\frac{n\varepsilon^2}{8}}. \quad (37)$$

Which is the result that we sought. This ensures that as we increase n and D , the distances between the embeddings of occupancy measures reflect the true MMD distance between them with a high probability.

B Calibrated Weighted PCA algorithm details

Our calibrated and weighted PCA variant addresses three critical requirements for effective specification of behavioral descriptors in QD optimization: finding meaningful behavioral variations, ensuring compatibility with QD archives, and adapting to the evolving population of solutions. Below, we detail each component and its motivation.

Given policies $\{\pi_1, \dots, \pi_m\}$ with embeddings $\Psi = [\psi^{\pi_1}, \dots, \psi^{\pi_m}]^T$ and fitness scores (estimated returns) $\{f_1, \dots, f_m\}$ our algorithm proceeds as follows:

Step 1: Score normalization. We normalize fitness scores to form a weight distribution:

$$\tilde{f}_i = \max \left(\frac{f_i - \min_j f_j}{\max_j f_j - \min_j f_j}, \frac{1}{m} \right) \quad (38)$$

$$w_i = \frac{\tilde{f}_i}{\sum_j \tilde{f}_j} \quad (39)$$

where the weights sum to 1. The $\frac{1}{m}$ term in Eq. 38 ensures a minimum contribution from each policy.

Motivation: While all policies provide information about the behavioral space, high-performing policies represent more successful strategies that we want to emphasize when discovering diverse behaviors. Low-performing policies often exhibit undesirable behaviors that should have less influence on our descriptors. The normalization ensures all policies contribute at least minimally while prioritizing those with higher fitness.

Step 2: Weighted PCA. We compute:

$$\mu = \sum_{i=1}^m w_i \psi^{\pi_i} \quad (\text{weighted mean}) \quad (40)$$

$$\hat{\psi}^{\pi_i} = \psi^{\pi_i} - \mu \quad (\text{centered embeddings}) \quad (41)$$

$$\tilde{\psi}^{\pi_i} = \sqrt{w_i} \hat{\psi}^{\pi_i} \quad (\text{weighted centered embeddings}) \quad (42)$$

We perform SVD on the weighted centered embeddings to obtain the top k principal components $\mathbf{P} \in \mathbb{R}^{D \times k}$.

Motivation: PCA offers several advantages for our context:

- It provides an affine transformation that preserves the geometry of the original embedding space, maintaining relative distances between policies up to scaling and translation.
- Unlike non-linear dimensionality reduction techniques, it doesn't introduce distortions that could misrepresent behavioral similarities.
- It requires no additional hyperparameters or iterative training procedures.
- The orthogonality of principal components ensures that each behavioral measure captures a distinct aspect of policy behavior.
- By weighting the PCA computation, we focus on capturing variations among high-performing policies.

Step 3: Calibration. We compute the 5th and 95th percentile quantiles of uncalibrated projections $\text{desc}(\pi) = \mathbf{P}^T(\psi^\pi - \mu)$ along each dimension:

$$\mathbf{q}_{\text{low}} = \text{quantile}(\{\text{desc}(\pi_i)\}, 0.05) \quad (43)$$

$$\mathbf{q}_{\text{high}} = \text{quantile}(\{\text{desc}(\pi_i)\}, 0.95) \quad (44)$$

The final transformation maps $[\mathbf{q}_{\text{low}}, \mathbf{q}_{\text{high}}]$ to $[-1, 1]^k$:

$$\mathbf{s} = \frac{2}{\mathbf{q}_{\text{high}} - \mathbf{q}_{\text{low}}} \quad (45)$$

$$\mathbf{c} = -\mathbf{1} - \mathbf{s} \cdot \mathbf{q}_{\text{low}} \quad (46)$$

$$\mathbf{A} = \text{diag}(\mathbf{s}) \mathbf{P}^T \quad (47)$$

$$\mathbf{b} = \mathbf{c} - \mathbf{A} \mu \quad (48)$$

(Operations in the first two lines are element-wise)

Motivation: Calibration addresses a practical challenge in QD optimization:

- PCA naturally produces dimensions with different scales based on variance, which would require dimension-specific archive bounds.
- Calibration standardizes all dimensions to a fixed range $[-1, 1]$, allowing the QD algorithm to use consistent archive bounds.
- This standardization enables more uniform coverage of the archive along each dimension, preventing the QD algorithm from disproportionately exploring directions with naturally higher variance.
- The 5th/95th percentile choice ensures that most solutions fall within the archive bounds.

Importantly, the calibration step preserves the affine nature of the transformation, combining the projection and scaling into a single linear operation \mathbf{A} with offset \mathbf{b} . This results in a computationally efficient mapping that maintains the essential geometric properties of the embedding space.

The final behavioral descriptor $\text{desc}(\pi) = \mathbf{A}\psi^\pi + \mathbf{b}$ adaptively identifies and scales the most significant behavioral dimensions, focusing on variations among high-performing policies while ensuring compatibility with fixed-bound QD archives.

C Details of CMA-MAE

Here we provide the pseudocode for both the initialization of CMA-MAE (Algorithm 2) as well as its update step (Algorithm 3). These were abstracted as function calls in Algorithm 1 in the main paper for the sake of clarity.

In these pseudocodes, note that the internal parameters of CMA-ES include a Gaussian “search” distribution that are used to sample candidate policy parameters (Line 4 of Algorithm 3) and are updated through CMA-ES (Line 17 of Algorithm 3). For a more detailed exposition of CMA-MAE, we refer the reader to [13].

Algorithm 2 CMA_MAE_Init

```

1: function CMA_MAE_INIT( $k$ )
2:   Input: Behavior space dimension  $k$ 
3:   Output: Empty archive  $\mathbb{A}$ , Optimization state QDState
4:   Initialize CMA-ES internal parameters: CMA_ES_State
5:   Initialize an empty archive  $\mathbb{A}$  ▷ Uniform grid over  $[-1.2, 1.2]^k$ 
6:   for all cells  $e$  in  $\mathbb{A}$  do
7:      $t_e \leftarrow \text{min\_objective}$  ▷ Acceptance threshold
8:   end for
9:   QDState  $\leftarrow$  (CMA_ES_State,  $\{t_e\}_{e \in \mathbb{A}}$ )
10:  return ( $\mathbb{A}$ , QDState)
11: end function

```

D Implementation details and hyperparameters

D.1 Environments

We use the latest versions of the environments available in Gymnasium [43] in our experiments:

- BipedalWalker-v3,
- Ant-v5,
- HalfCheetah-v5,
- Hopper-v5,
- Swimmer-v5,
- Walker2d-v5.

Algorithm 3 CMA_MAE_Step

```
1: function CMA_MAE_STEP( $\mathbb{A}$ , QDState, desc)
2:   Required Hyperparameters: learning rate  $\alpha$ , batch size  $\lambda$ 
3:   for  $i = 1, \dots, \lambda$  do
4:     Sample candidate:  $\theta_i \sim \mathcal{N}(\theta_{\text{QDState}}, \Sigma_{\text{QDState}})$ 
5:     trajectories  $\leftarrow \text{collect\_rollouts}(\theta_i)$ 
6:      $f \leftarrow \text{mean\_return}(\text{trajectories})$  ▷ Fitness
7:     Compute  $\psi$  according to Eq. 6 from trajectories
8:     BD  $\leftarrow \text{desc}(\psi)$ 
9:      $e \leftarrow \text{calculate\_cell}(\mathbb{A}, \text{BD})$  ▷ Locate corresponding cell from the archive
10:     $\Delta_i \leftarrow f - t_e$  ▷ Improvement over the cell's threshold
11:    if  $f > t_e$  then
12:      Replace the current occupant of cell  $e$  in the archive  $\mathbb{A}$  with  $\theta_i$ 
13:       $t_e \leftarrow (1 - \alpha)t_e + \alpha f$ 
14:    end if
15:  end for
16:  Rank  $\theta_i$  by  $\Delta_i$ 
17:  Adapt CMA-ES parameters based on improvement rankings  $\Delta_i$ 
18:  return updated  $\mathcal{S}$ 
19: end function
```

D.2 Network architecture

All QD-based methods (AutoQD, Aurora, LSTM-Aurora, and RegularQD) use identical policy architectures: a neural network with two hidden layers of 128 units each and tanh activation functions. These networks employ a Toeplitz structure, which constrains the weight matrices such that all entries along each diagonal share the same value [6]. This constraint enforces parameter sharing and reduces the search space.

SMERL uses a similar network architecture but with ReLU activations and without the Toeplitz constraint. Since SMERL employs gradient-based RL optimization, the Toeplitz structure is not necessary. We use ReLU activations to keep consistency with the author's hyperparameters and the open source implementations.

DvD-ES uses the authors' provided implementation, which employs MLPs with two hidden layers of size 32.

D.3 QD algorithm configuration

All methods utilize the standard Pyribs [41] implementation of CMA-MAE [13] as the underlying QD algorithm. They employ grid archives that are discretized to 10 cells along each dimension and use 5 emitters with different initial step sizes of $\{0.01 \times 2^i\}_{i=1}^5$. The rest of the configuration is presented below.

Table 3: Common QD algorithm parameters shared across all methods

Parameter	Value
Number of CMA-ES Instances	5
Initial Step Size (σ_0)	$\{0.01 \times 2^i\}_{i=1}^5$
Batch Size	64
Restart Rule	100 iterations
Archive Learning Rate	0.01
Total Iterations	500
Evaluations per Policy	5

D.4 AutoQD

Our proposed method uses Random Fourier Features (RFF) to map trajectories/policies into embeddings and progressively refines a measure map during optimization using calibrated weighted PCA to convert policy embeddings into low-dimensional behavior descriptors. The embedding map normalizes the observations based on the trajectories that it observes throughout its lifetime.

Table 4: AutoQD-specific parameters

Parameter	Value
<i>RFF Embedding</i>	
Embedding Dimension	100
State Normalization	True
Kernel Width	$\sqrt{\text{state dim} + \text{action dim}}$
Discount Factor (γ)	0.999
<i>Measure Map</i>	
Measures Dimension	4
Update Schedule	[20, 50, 100, 200, 300]

The update schedule indicates the iterations at which the measure map is refined using the current archive.

D.5 Aurora

Aurora learns a behavioral characterization using an autoencoder that reconstructs states.

Table 5: AURORA parameters

Parameter	Value
<i>Encoder Architecture</i>	
Mapping	$\mathcal{S} \rightarrow \mathbb{R}^4$
Hidden Layers	[64, 32]
Latent Dimension	4
<i>Decoder Architecture</i>	
Mapping	$\mathbb{R}^4 \rightarrow \mathcal{S}$
Hidden Layers	[32, 64]
<i>AutoEncoder Training</i>	
Max Epochs	50
Learning Rate	0.001
Batch Size	64
Validation Split	0.2
Early Stopping Patience	10
Update Schedule	[20, 50, 100, 200, 300]

At each iteration, the autoencoder is trained for a maximum of 50 epochs on 80% of all data. A validation loss is computed using the remaining 20% and if it does not decrease for 10 consecutive epochs, the training can stop earlier.

D.6 LSTM-Aurora

This variant of AURORA uses an LSTM-based architecture to encode full trajectories. The encoder maps sequences of states to hidden states. The last hidden state of a trajectory is mapped to a latent vector (the behavioral descriptor). The decoder maps this latent back to a hidden state vector and reconstructs the trajectory starting with this hidden state and using teacher forcing.

The trajectory sampling frequency of 10 means that every 10th state in a trajectory is used for encoding, following the authors’ implementation.

Table 6: LSTM-Aurora parameters

Parameter	Value
<i>Encoder-Decoder Architecture</i>	
Type	LSTM
Hidden Dimension	32
Latent Dimension	4
Hidden-to-Latent Map Type	Linear
Latent-to-Hidden Map Type	Linear
Teacher Forcing	True
Trajectory Sampling Frequency	10
<i>AutoEncoder Training</i>	
Epochs	50
Learning Rate	0.001
Batch Size	64
Validation Split	0.2
Early Stopping Patience	10
Update Schedule	[20, 50, 100, 200, 300]

D.7 RegularQD

The baseline RegularQD method uses handcrafted behavioral descriptors specific to each environment. For all of the environments except Swimmer, these are the foot-contact frequencies which are commonly used in literature. For Swimmer, we use three descriptors that measure angular span (i.e., how much the joints bend), phase coordination (i.e., how well the joints coordinate), and straightness (i.e., how straight the trajectory is).

D.8 SMERL

Our implementation of SMERL is based on an open source implementation, modified slightly to make it compatible with the latest version of the environments and to add parallelization. Other than increasing the size of network’s hidden layers (two hidden layers of size 128), doubling the number of skills to 10, and increasing the total training steps to 1.6×10^7 total timesteps, we keep the default hyperparameters.

D.9 DvD-ES

We use the DvD-ES implementation provided by the authros (link) with slight modifications to make it compatible with the latest versions of the environments. Other than the number of policies (we use 10) we keep the default hyperparameters.

D.10 Evaluation

In Sec. 4.2 we stated that the Vendi Score (VS) relies on a positive-definite similarity kernel. For this purpose, we use the Gaussian (RBF) kernel, defined for a pair of embeddings \mathbf{x} and \mathbf{y} as:

$$K = \exp(-\gamma \|\mathbf{x} - \mathbf{y}\|^2) \quad (49)$$

To select an appropriate value of γ , we adopt a variant of the *median heuristic* [18], which sets

$$\gamma = \frac{\ln 2}{\text{median}(\|\mathbf{x}_i - \mathbf{x}_j\|^2)}, \quad (50)$$

where the median is computed over the pairwise squared distances between all policy embeddings. This choice ensures that two embeddings separated by the median distance will have a similarity of $K = 0.5$, offering an intuitive scaling of the kernel. To reduce computational overhead for methods that generate a large number of policies, we randomly subsample up to 1000 embeddings when computing the median distance.

Finally, we emphasize that this similarity kernel is distinct from the one used to construct the random Fourier feature (RFF) embeddings described in Sec. 3.1.

D.11 Computational Resources

All of our experiments were conducted on local machines with an *AMD Ryzen Threadripper PRO 5995WX 64-Cores* CPU, 64GB of memory and either an *NVIDIA GeForce RTX 4090* or *NVIDIA GeForce RTX 3090* GPU. Each training run for any of the algorithms took ≤ 3 hours except the experiments for the SMERL baseline which took around 1 day each. Furthermore, the evaluation of each population took ≤ 1 hours.

E Effect of embedding and behavior space dimensions

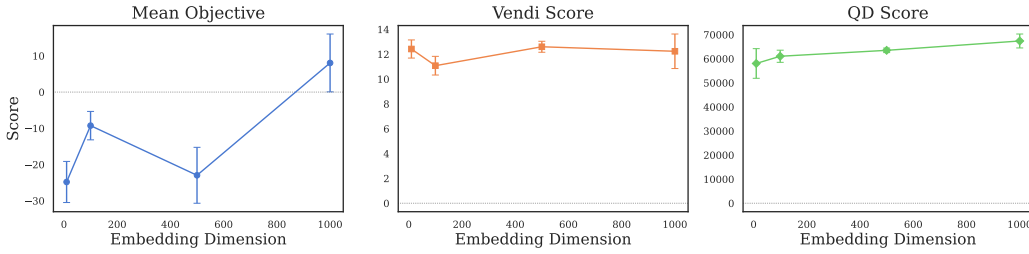


Figure 4: Ablating RFF embedding dimension on BipedalWalker. The plot report mean values over 3 random seeds with bars indicating standard errors.

We perform two ablation studies to investigate how the dimensionality of (i) the behavior descriptors and (ii) the random Fourier feature embeddings affects performance. All experiments are conducted on the BipedalWalker environment using three different random seeds. We report the mean and standard error (shown as error bars) for three key metrics:

Mean Objective. The average of the objective values across all policies found by the algorithm with a given configuration. It represents the overall quality of discovered solutions.

Vendi Score. A measure of behavioral diversity. Recall that it can be interpreted as the effective population size.

QD Score. The Ground Truth QD score introduced as in the main paper. It captures both the quality and the human-interpretable diversity of the discovered policies.

Note that quality-weighted Vendi Score (qVS) used in the main paper is just the product of the mean objective, normalized and scaled to be in $[0, 1]$, with the raw Vendi score. Here we report the raw Vendi score and the unnormalized mean objectives separately to provide a clearer picture of quality and diversity independently.

For the behavior descriptors, we vary the dimensionality of the measure space from 1 to 4. Fig. 5 presents the results which show a consistent improvement in both the QD score and the Vendi score as the dimensionality increases. In contrast, the mean objective value decreases with higher descriptor dimensionality. This suggests that as the behavior space becomes more complex, the fraction of high-quality solutions among all discovered solutions declines. This trend is intuitive: if we assume that a fixed proportion $\varepsilon \in (0, 1)$ of behaviors along each axis are high-performing, then the overall fraction of high-quality solutions decreases exponentially with the number of descriptor dimensions. Additionally, lower-dimensional behavior spaces may be easier for the underlying CMA-ES optimizer to search effectively for high-quality solutions.

For the embeddings, we vary the number of random Fourier features from 10 to 1000, evaluating configurations with 10, 100, 500, and 1000 dimensions. Fig 4 presents the results which suggest that performance is relatively robust to this hyperparameter. While our main experiments use 100-dimensional embeddings, even with as few as 10 features, AutoQD achieves competitive performance in terms of both quality and diversity.

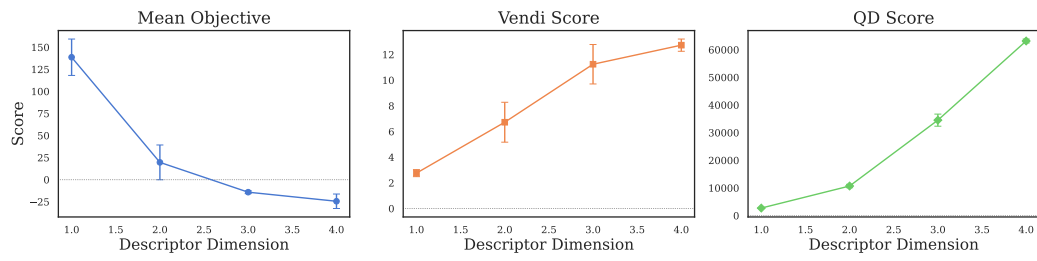


Figure 5: Ablating BD’s dimension on BipedalWalker. The plot report mean values over 3 random seeds with bars indicating standard errors.